Matemática Contemporânea, Vol. 22, 97–112
http://doi.org/10.21711/231766362002/rmc227

MAGNETOCARDIOGRAPHIC LOCATION OF ROTATING SPIRAL ELECTROCHEMICAL WAVES

R. W. dos Santos * **D. Marchesin** † **B. Gundelach** ‡
J. Valério §

Abstract

We describe and compare two inverse algorithms to recover the center and other parameters describing reentry currents associated to atrial flutter. Noninvasive measurements at different locations away from the atrial tissue are assumed to be recorded in the form of magnetic field time series generated by the reentry current. Signal processing in time domain and a least-square procedure are used to identify and locate the reentry current. Using synthetic experiments, we show that a new method employing (i) a continuously measured atrial electric signal to synchronize the magnetic measurements and (ii) a three-dimensional description of the reentry pattern leads to a considerably more robust recovery method, as compared to a former method that did not employ the electric signal. Our hope is to improve this method to provide a basis for a noninvasive and inexpensive but accurate diagnostic tool for locating reentry current patterns.

1 Introduction

Cardiac arrhythmia known as atrial flutter is usually associated with a reentrant excitation of atrium cells. In such a situation, instead of the normal activation originating at the right atrium sinus node and propagating toward the ventricles, the electrical activity starts to rotate continuously within the atrium. For drug intolerant patients, current therapy consists of locating the reentrant excitation and interrupting its path by application of radio-frequency energy, the so

*Supported by CAPES Doctoral Fellowship
†Supported by CNPq under Grants 520725/95-6 and 300204/83-3; MCT under Grant PCI 650009/97-5; FINEP under Grant 77.97.0315.00; FAPERJ under Grant E-26/150.936/99
‡Supported by MCT under Grant PCI 650009/97-5
§Supported by CNPq under Grant 520725/95-6.

called ablation technique. Both procedures (anatomical location and ablation) involve catheter invasion and X-ray exposition [6]. A first step towards a non-invasive therapy consists of locating and characterizing the reentrant current noninvasively. Recent studies point to an emerging technique called magneto-cardiography, or simply MCG, which may cope with such a task. It is known that electrical data, such as ECG, allow detection of the arrhythmia pathology but cannot provide enough information to locate the exact reentry path. Better results are achieved when measuring magnetic activity from different spatial locations above the heart and combining magnetic and electric information. The drawback of such MCG systems lies in the high cost of the array of magnetic detectors.

A new MCG system is now under evaluation [4]. It is designed to be cost effective and yet to provide enough information for recovering flutter characteristics and location. It consists of a single mobile magnetic detector (a SQUID gradiometer), used to register magnetic activity at several positions over the heart. Taking advantage of the quasi-periodicity in time of the reentry current, these records at different locations may then be combined and processed in order to provide essentially the same information that would be obtained with multiple detectors. This is what we call the pre-processing phase. Following this phase, the pre-processed data is further analyzed by more sophisticated algorithms that will finally retrieve physical and geometric flutter parameters, such as location. This is the inverse problem phase. This MCG system replaces expensive multiple detector systems by a single mobile detector powered by sophisticated mathematical tools. Since the magnetic measurements are obtained by a single mobile detector at different positions, they are data for different time periods, which are periodic functions recorded with different phases, *i.e.* the records are asynchronous. Of course, all the magnetic records are supposed to have the same period, the reentry current period. In previous works [1], a 2-D asynchronous inverse problem algorithm was presented in the context of a special experiment using animal atrial tissue. The reentry current mathematical model used in that implementation was two-dimensional (2-D) and the inverse problem solver was developed to deal with asynchronous data. A simple 2-D model for the reentry current seemed to be adequate since the animal heart tissue was arranged in a planar configuration during the experiments.

In this paper we propose, implement, test and compare synthetically two new and improved inverse problem algorithms: a 3-D algorithm that deals with

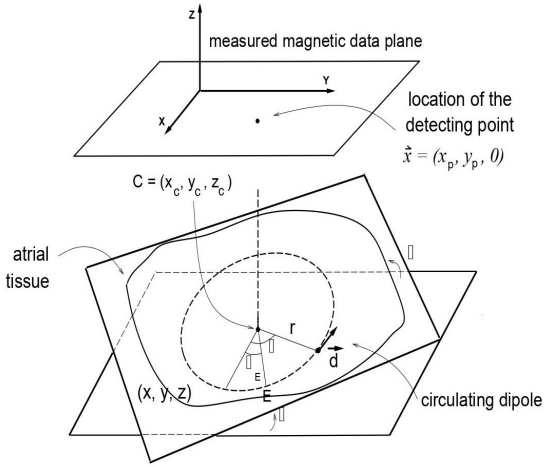

Figure 1: 3-D circulating current dipole model

asynchronous data and a 3-D algorithm that has been further improved to deal with synchronous data. Both algorithms extend the reentry current model to a more general three dimensional (3-D) space setup, a step towards future noninvasive human experimentation. The magnetic data synchronization is achieved using electrical measurements. We tested both algorithms and compared their performance using synthetic data. In our synthetic experiments both methods achieved very good results but the synchronous version was much more robust.

The remainder of this paper is organized as follows. The next section describes the 3-D circulating dipole model we use for the reentry current. Section 3 describes the asynchronous and synchronous versions of the inverse problem implementation. Section 4 presents the graphical environment and programs developed for the pre-processing and the inverse problem solving phases. Section 5 presents and discusses our numerical experiments. Finally, Section 6 presents our conclusions and discusses work we intend to do in the near future.

2 A 3-D model for reentry currents

Our starting point is the assumption that the electrical activity may be represented by a simple model: a current dipole describing a circular path and

pointing tangentially within the planar piece of atrial tissue. Experiments with rabbit heart tissues [7] have indeed characterized the rotating pattern of propagation as the underlying mechanism of such arrhythmias. The magnetic field $\vec{B}$ at a point $\vec{x}_p$ in space, generated by a dipole $\vec{d}$, is given by Biot-Savart's Law:

$$\vec{B} = \frac{\mu_0}{4\pi} \frac{\vec{d} \times \vec{x}}{|\vec{x}|^3}, \tag{1}$$

where $\vec{x}$ is the distance between the measuring point $\vec{x}_p$ and the dipole position $\vec{x}_d$:

$$\vec{x} = (x_p, y_p, 0) - (x_d, y_d, z_d). \tag{2}$$

The dipole vector $\vec{d}$ is characterized by dipole intensity s and the unit direction vector obtained from the time derivative of the position vector $\vec{x}_d$:

$$\vec{d} = s \frac{\dot{\vec{x}}_d}{|\dot{\vec{x}}_d|}. \tag{3}$$

As shown in Fig. 1, the continuous rotation of the dipole on a circle with radius r and center $\vec{x}_c$ is described by angle θ, on plane P. θ increases linearly with time. Plane P has normal vector equal to $\vec{N} = (-\sin\alpha\cos\beta, -\sin\beta\sin\alpha, \cos\alpha)$, where the angle α describes the rotation of the plane P around the y axis and the angle β describes the rotation of P around the z axis, as shown in Fig. 1. If $\alpha = \beta = 0$, P would be positioned on the horizontal plane, as in the 2-D model studied in [1]. After some calculations we can write the dipole position vector $\vec{x}_d$ as:

$$\vec{x}_d(\theta) = \vec{x}_c + r(\cos\beta\cos\alpha\cos\theta - \sin\beta\sin\theta, \sin\beta\cos\alpha\cos\theta + \cos\beta\sin\theta, \sin\alpha\cos\theta). \tag{4}$$

We calculate $\vec{d} \times \vec{x}$ using Eqs. (4), (3) and (2). Extracting the vertical component in Eq. (1), we can write the magnetic field at position $\vec{x}_p$ as a function of θ:

$$B(\theta) = \frac{s}{|\vec{x}|^3} \left[r\cos\alpha - u\cos\theta - v\cos\alpha\sin\theta \right], \tag{5}$$

where $u = (x_p - x_c)\cos\beta + (y_p - y_c)\sin\beta$, $v = -(x_p - x_c)\sin\beta + (y_p - y_c)\cos\beta$ and $\vec{x}$ is determined from Eq. (2).

Eq. (5) completes the very simple model for the magnetic field generated by cardiac reentry currents proposed by [1]. From now on we call it simply the circulating dipole model and use it to recover the dipole radius r, center

position $\vec{x}_c$, the α and β plane angles and the intensity s, in the hope that this information will agree with the reentry current characteristics and location. In the next section we describe our data pre-processing and inverse problem algorithms.

3 The inverse problem

We apply least square procedures for retrieving the relevant dipole parameters enumerated in Section 2. Creating cost functions that compare measured magnetic data and simulated data based on the circulating dipole model, our algorithms aim at finding the best dipole model parameters to minimize the difference between the recorded and the simulated data.

We developed two algorithms that differ in the way measured magnetic data are used and therefore employ different cost functions. Otherwise, both apply the same least square procedure, the Nelder-Mead [3], which is known to be a robust and reliable simplex search method. Another feature in common is that both algorithms work with frequency-domain data. Thus, instead of using time-dependent data, Fourier coefficients of the time series data are used. Since our data are essentially periodic, each time series can be represented by a Fourier series with coefficients as below:

$$(\widehat{C}_{p,n}, \widehat{S}_{p,n}) \equiv \frac{1}{T}\int_0^T (\cos(nt), \sin(nt))\widehat{B}_p(t)\, dt, \tag{6}$$

where $p = 1, 2, \ldots, positions$, is the index of the magnetic measurements taken at different positions, and $n = 0, 1, 2, 3, \ldots$ is the Fourier harmonic index, T is the reentry current period and $\widehat{B}_p$ is the magnetic time series itself.

Although theory only ensures the time-frequency equivalence with infinitely many harmonics, we show in Section 5 that we may reliably reconstruct the signal with very few harmonics, saving substantial computing effort. In addition, many filtering and pre-processing methods may be applied on the frequency-domain data in order to reduce undesirable environmental noise introduced during measurement, as we show in Section 4. In the future, this feature will be very helpful when using inexpensive high critical temperature SQUIDs.

In order to simulate the reentry current we use the dipole model described in Section 2. Combining Eqs. (5) and (6), it follows that the simulated harmonics

are given by:

$$(C_{p,n}, S_{p,n})(\varphi_p, \vec{dip}) \equiv \frac{1}{2\pi} \int_0^{2\pi} (\cos(n\theta), \sin(n\theta)) B_p(\theta + \varphi_p, \vec{dip})\, d\theta, \tag{7}$$

where p and n are the indices of the position detector and the harmonic number as before, B_p is the magnetic flux calculated by Eq. (5) and the vector $\vec{dip}$ contains the dipole parameters of the circulating magnetic dipole model:

$$\vec{dip} = (r, s, x_c, y_c, z_c, \alpha, \beta). \tag{8}$$

The unknown phase φ is included in the equations above in order to allow alignment in time of the simulated data B with the timing record $\widehat{B}$. In addition, due to the serial magnetic detection procedure, each position record possesses its own phase φ_p. The two algorithms described in Sections 3.1 and 3.2 differ in the processing of these phases.

3.1 The asynchronous scheme

Since the magnetic signal B is periodic, its R.M.S. energy $||B(\varphi)||^2 \equiv \frac{1}{2\pi} \int_0^{2\pi} B(\theta + \varphi)^2\, d\theta$ does not depend on the phase φ. Similarly, the energy associated with the n-th harmonic

$$|A_{p,n}(\varphi)|^2 = |C_{p,n}(\varphi)|^2 + |S_{p,n}(\varphi)|^2 \tag{9}$$

does not depend on the phase φ either. When $C_{p,n}$ and $S_{p,n}$ are obtained from Eq. (7), we use $A_{p,n}$ for the simulated data; when $C_{p,n}$ and $S_{p,n}$ are obtained from recorded data given by Eq. (6), we use $\widehat{A}_{p,n}$.

Based on these considerations, the following asynchronous scheme was developed:

- Pre-processing phase: here the Fourier coefficients for the magnetic records are generated using the FFT [5] algorithm and several other filtering techniques in order to extract the harmonics as described in Eq. (6).

- Inverse problem phase: we apply the simplex search algorithm mentioned before to minimize the following cost function:

$$\mathcal{F}(\vec{dip}) = \frac{1}{K} \sum_{p,n} |\widehat{A}^2_{p,n} - A^2_{p,n}(\vec{dip})|^2, \tag{10}$$

where K is a normalization factor, p and n indicate the detector positions and the harmonic number as before, the vector $\vec{dip}$ carries the dipole parameters of interest as described by Eq. (8), and $\widehat{A}_{p,n}$ and $A_{p,n}$ are respectively the recorded and simulated harmonic R.M.S. norm as in Eq. (9).

Examining the cost function in Eq. (10), we notice that the scheme does not align, or synchronize, any of the measured and simulated signals, since it does not use information contained in the phases φ_p. It analyzes the spatial distributed information as it was recorded, asynchronously. We can already suspect that this algorithm cannot fully replace a multiple detector MCG system, where data is recorded synchronously and thus both spatial and temporal information are available. Here the time correlation between the samples is lost. Mathematical analysis also supports this claim. Indeed, using frequency-domain information contained in $A_{p,n}$ instead of using both $C_{p,n}$ and $S_{p,n}$, one is not able to reconstruct reliably the time-domain signal (except in symmetric and atypical cases where either $C_{p,n}$ or $S_{p,n}$ vanishes). The method we propose now solves this problem.

3.2 The synchronous scheme

As stated before, we need a method that handles the various (and unequal) phases φ_p which appear in Eq. (7). In fact, these phases originate from three sources of asynchronism. The first one comes from slow frequency decrease observed in animal experiments. The second one comes from the measurement procedure, which is sequential and therefore adds different phases to different record positions. The third source is due to the mathematical dipole model we proposed, *i.e.* the phase difference between the simulated data and the real recorded data. Thus, we need first to synchronize the spatially distributed recorded data in order to simulate a multiple detector system. Then, we align the simulated and the recorded data. To accomplish the first step we use a natural clock, the heart. Measuring without interruption the voltage of an electrode placed at a fixed point of the atrial tissue while measuring magnetic activity at every position, the electric signal can be used as a common clock. For each position, we simultaneously record two signals, the magnetic signal $\widehat{B}_p$ and the electrical signal $\widehat{E}_p$. This information is enough to synchronize all recorded magnetic signals. Once this is done, a new cost function is applied during the

minimum search procedure. This cost function carries a new parameter, the phase between the recorded and the simulated data. Below we describe the details of the synchronous scheme:

- Pre-processing phase: again the Fourier coefficients for both $\widehat{E}_p$ and $\widehat{B}_p$ records are generated by using an FFT algorithm and several other filtering techniques. The recorded data are synchronized in the frequency-domain. We extract the fundamental harmonic phase φ_{E_p} of each $\widehat{E}_p$ record by: $\cos\varphi_{E_p} = \int_0^T \widehat{E}_p(t)\cos\omega t\,dt$ and $\sin\varphi_{E_p} = \int_0^T \widehat{E}_p(t)\sin\omega t\,dt$. The magnetic records are then shifted by adding the corresponding phase φ_{E_p} to all of its harmonics $\widehat{C}_{p,n}$ and $\widehat{S}_{p,n}$ (calculated by Eq. (6)):

$$\begin{pmatrix} \overline{C}_{p,n} \\ \overline{S}_{p,n} \end{pmatrix} = \begin{pmatrix} \cos(n\varphi_{E_p}) & \sin(n\varphi_{E_p}) \\ -\sin(n\varphi_{E_p}) & \cos(n\varphi_{E_p}) \end{pmatrix} \begin{pmatrix} \widehat{C}_{p,n} \\ \widehat{S}_{p,n} \end{pmatrix} \tag{11}$$

  Executing this procedure for each recorded pair $\widehat{E}_p$ and $\widehat{B}_p$, all magnetic signals $\overline{C}_{p,n}$ and $\overline{S}_{p,n}$ end up synchronized.

- Inverse problem phase: we apply the Nelder-Mead simplex search algorithm to minimize the following cost function:

$$\mathcal{F}(\varphi, \vec{dip}) = \frac{1}{K}\sum_{p,n} |\overline{C}_{p,n} - C_{p,n}(\varphi, \vec{dip})|^2 + |\overline{S}_{p,n} - S_{p,n}(\varphi, \vec{dip})|^2, \tag{12}$$

  where K is a normalization factor, p and n indicate the detector position and the harmonic number as before, the vector $\vec{dip}$ carries the dipole parameters of interest as described by Eq. (8), and the phase φ takes into account the time lag between the simulated and real data and is used in $C_{p,n}$ and $S_{p,n}$ as shown in Eq. (7). Finally, the harmonics $\overline{C}_{p,n}$ and $\overline{S}_{p,n}$ are the measured magnetic data synchronized by Eq. (11).

4 Computer implementation

We implemented the previous algorithm phases, pre-processing and inverse problem, in the Matlab 6.0 environment. Pre-processing is done using a graphical and user-friendly interface program, depicted in Fig. 2, offering many useful signal processing options to help the user in tasks such as harmonics extraction, filtering and data synchronization. The input may be a file containing the

measured magnetic B_p and electric E_p time series. Once this file is loaded, the FFT's of the signals are computed. In the current version, the signals are processed by two filters, a DC and a Hanning window filter. The DC component is removed because it cannot be reliably measured by the current DC SQUID laboratory instrument. (This is unfortunate, since earlier studies [1] indicate that the DC harmonic contains more information than the other harmonics.) The harmonics can be automatically extracted from the FFT signal or may be mouse-selected by the user. The user can also choose whether synchronization between the E_p and B_p signals is desired or not.

The inverse problem implementation utilizes a flexible Matlab function that we call "Optimize". It applies the Nelder-Mead simplex search method to the cost functions described in Eqs. (10) or (12). It reads the harmonic file generated by the pre-processing program and writes out the best dipole $\vec{o}ut$ and the cost achieved through optimization. Its interface provides control of parameters such as: the dipole $\vec{i}ni$ initial estimate, the number of detector positions np to be considered, the number of harmonics nh to be used, and the termination tolerance tol for the simplex search method, among others. In addition, the user may choose whether to use the synchronous or the asynchronous cost functions.

5 Numerical results

Both asynchronous and synchronous algorithms were tested using synthetic data; we will use real laboratory data in the future. Using Eq. (5), the magnetic time series B_p were generated for 21 different detector positions. We used the following synthetic dipole description:

$$\begin{aligned} \vec{min} &= (r, s, x_c, y_c, z_c, \alpha, \beta) \\ &= (0.9\text{cm}, 3.0\text{w/m}^2, 0.3\text{cm}, 0.8\text{cm}, 1.9\text{cm}, 1.0\text{rad}, 0.4\text{rad}), \end{aligned}$$

for a 4.5 Hz frequency of 4.5Hz and added phase $\varphi = 1.1$rad, simulating the time lag between the measured and simulated signals. The detector positions $\vec{x}_p$ are the same as those used in previous animal experiments [4]. They lie on the x axis or on the y axis, in a horizontal plane lying two centimeters above the atrial tissue, forming a cross pattern with equally spaced points in a range from -2.5cm to 2.5cm. We simulated the electric signals E_p with a simple cosine function with the same frequency as that of the circulating dipole, since it is used only for synchronization. We then used the pre-processing program to

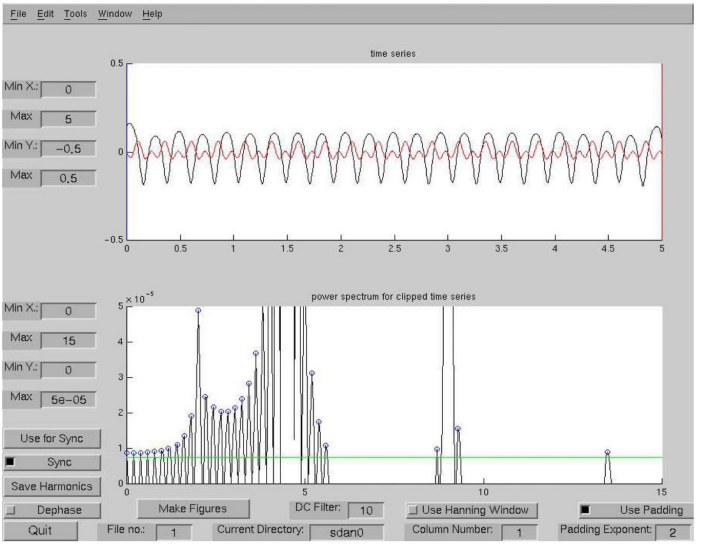

Figure 2: Pre-processing Matlab graphical environment

extract up to 6 harmonics from the time series data and to synchronize them with the E_p signals, as described in the previous sections. We generated two files with the pre-processing program. One of the files contains extracted but not synchronized harmonics that are used in the asynchronous algorithm described in Sec. 3.1. The other file contains synchronized harmonics that are used in our synchronous scheme as described in Sec. 3.2. All tests were carried out on a Pentium III 700MHz processor with 256MBytes of memory running in a Linux operating system.

In our first test we generated 20 random initial dipole guesses, which are different but have the same R.M.S. distance from the vector $\vec{min}$ described in Eq. (13), *i.e.* $||\vec{min} - \vec{ini}|| = 2.5$. We use them in the "Optimize" program with input parameters (described in Sec. 4) $nh = 6$, $np = 21$ and $tol = 1.0\text{e-}04$. Both asynchronous and synchronous algorithms rendered dipole $\vec{out}$ parameters very close to the original ones in $\vec{min}$. Choosing among the 20 runs the one that attained the smallest cost, it follows that the asynchronous and synchronous methods achieved errors of 7.8e-05 and 1.3e-05 respectively, where we used again the R.M.S. norm to compute the error, *i.e.* $error = ||\vec{min} - \vec{out}||$. We hope

that this procedure simulates a typical application usage, where the user runs our algorithm with a few initial guesses and then chooses the best solution as indicated by our algorithm. It is important to remember that the chosen dipole $\vec{out}$ is not necessarily the one with minimum error because the user usually does not know the correct dipole solution. Therefore we use the one with minimum cost in our tests. While the error attained by the synchronous algorithm is 6 times smaller than the error achieved by the asynchronous algorithm, the latter is faster. Its average running time was 60 seconds and 1600 steps, while the synchronous method algorithm took an average time of 88 seconds and 2300 steps per run. However, the computing cost is a secondary consideration.

We examine next the effect of using different numbers of positions np, and of harmonics nh used in our inverse problem schemes. Again 20 random initial dipole guesses with fixed R.M.S. distance from $\vec{min}$ are used. Letting nh vary from 1 to 6 and np vary from 1 to 21, we end up with 21x6x20 = 2520 tests per method. As before, for each (np, nh) pair we select the best $\vec{out}$ dipole by choosing the one that attains the smallest cost. In order to understand better the effect of the harmonic and position numbers, we show two 2-D plots instead of a single 3-D plot. Thus, to asses the np effects we sum up all errors in the variable nh, *i.e.* $error(np) = \sum_{nh=1}^{6} error(np, nh)$, and show them in Fig. 4. The same was done in order to understand how nh affects our schemes, $error(nh) = \sum_{np=1}^{21} error(np, nh)$, as shown in Fig. 3. In both figures there are two bars per point. The left bar shows the asynchronous algorithm errors and the right one the synchronous values.

We see in Fig. 3 that both methods experience great error reduction when more than one harmonic is used. On the other hand, using more than 3 harmonics we notice that the magnitude of the errors starts to oscillate. Therefore, we conclude that a few harmonics are enough for efficiently recovering the dipole parameters. In addition, comparing the asynchronous and synchronous bars we verify that the synchronous method achieves better results than the asynchronous one.

The first important information we can extract from Fig. 4 is that indeed many magnetic detector positions are necessary to recover properly the reentry current parameters. The errors drop substantially when more than 3 positions are used in the synchronous algorithm or when more than 6 positions are used in the asynchronous algorithm. Thus, the synchronous algorithm can recover the dipole parameters with fewer measurements. This is a great advantage in

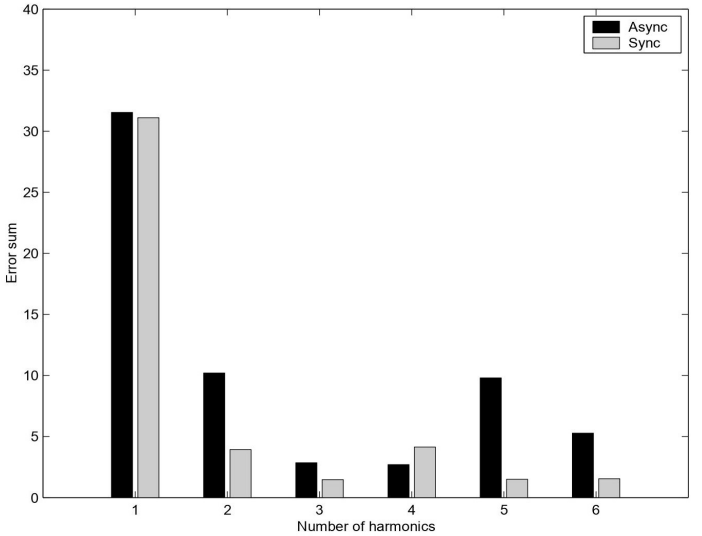

Figure 3: Harmonic numbers effect

practice. Comparing the error values, it again follows that the synchronous scheme outperforms the asynchronous scheme.

Finally, we plot slices of the asynchronous and synchronous cost functions given in Eqs. (10) and (12), using 6 harmonics and 21 detector positions, for the same synthetic generated dipole $\vec{min}$. Figures 5 and 6 illustrate how the following dipole parameters affect the cost functions: the dipole intensity s, the dipole center y_c and x_c and the angle β. The cost function is evaluated for each of these parameters, considering the other parameters fixed as the $\vec{min}$ values in terms of the varying parameter. We see that all figures present a single global minimum point as expected. But a closer examination of the asynchronous plots (Fig. 5) shows the presence of many other undesirable local minimum points for each of the variables y_c, x_c and β. Spurious minima in some of the variables slow down the search of the global minimum. The synchronous cost function (Fig. 6) has a more favorable shape. For instance, the shape of the intensity s is similar to a parabola, the ideal shape for minimum search methods. Finally, combining the cost function plots and the numerical results previously described we confirm our statement in Sec. 3: the synchronous scheme is more robust

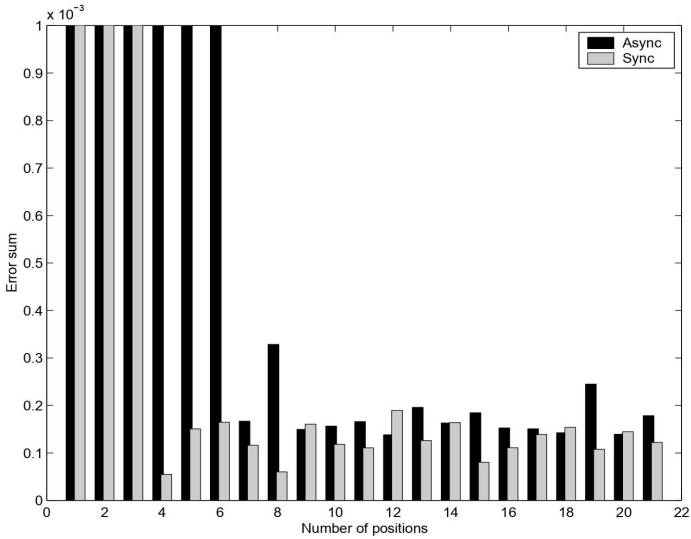

Figure 4: Position numbers effect

than the asynchronous scheme.

6 Conclusions and future work

In this paper we presented two new 3-D inverse problem algorithms for recovering atrial flutter characteristics using magnetocardiographic data: an asynchronous and a synchronous algorithm. Both algorithms extend the reentry current model previously presented [1] to a more general three dimensional (3-D) space setup, a step towards noninvasive future human experimentation. In addition, further improvements were made regarding magnetic data synchronization, resulting in what we called the synchronous scheme. We tested both algorithms and compared their performance using synthetic data. In our synthetic experiments both methods achieved good results, but the synchronous algorithm was much more robust than the asynchronous one. We hope that the single mobile magnetic detector setup described in [4] associated with mathematical tools based on our synchronous algorithm will provide a basis for a noninvasive and inexpensive but accurate diagnostic tool for locating cardiac

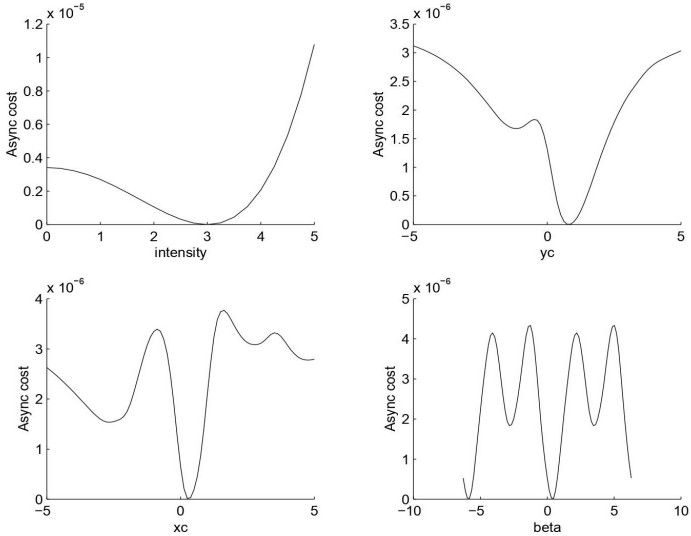

Figure 5: Asynchronous cost function

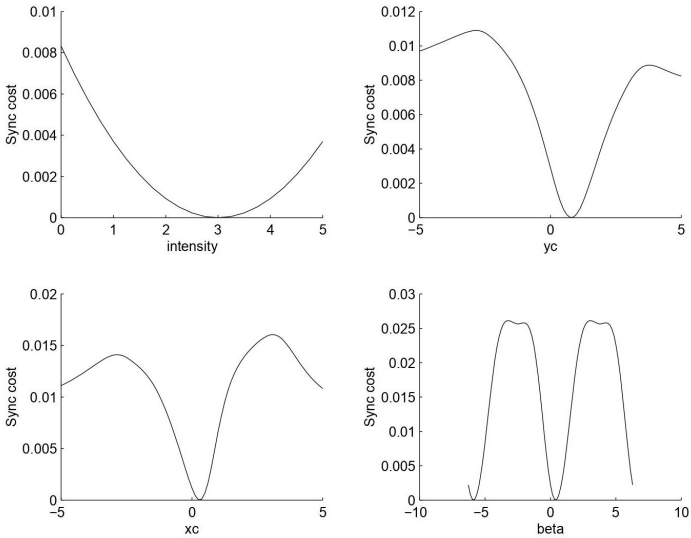

Figure 6: Synchronous cost function

reentry currents.

Our next step is the validation of our techniques using laboratory data recorded from animal experiments. Experimental setup to obtain reliable data is still being prepared. In order to proceed towards human experimentation, we have to improve our filtering techniques to remove the QRS heart signal. The animal atrial tissue experiments were designed precisely to eliminate the QRS signal, facilitating the development of recovery algorithms without having to deal with this complication. In addition, we are currently implementing a more sophisticated reentry current model employing evolutionary partial differential equations [2] related to a planar Hodgkin-Huxley model. This model will provide a better understanding of the properties underlying cardiac flutter pathology and validate the effectiveness of the simple circulating current dipole model. In the future, we hope to tackle a considerably more difficult problem, ventricular reentry currents associated to sudden death in clinical patients.

Acknowledgments. We thank Paulo Costa Ribeiro and Elisabeth Costa Monteiro for useful discussions and Bradley Plohr and Andrew Marchesin for the first version of the Matlab codes.

References

[1] Brio, M.; Marchesin, D.; Monteiro, E. C.; Bruno, A. C.; Ribeiro, P. C., *Inverse magnetocardiography for reentry currents*, Cheryl J. Aine, Yoshio Okada, Gerhard Stroink, Stephen J. Swithenby, Charles C. Wood. Advances in Biomagnetism Research, Volume I: Instrumentation; Forward and Inverse Problems; Magnetocardiography, 1997.

[2] Karma, A.; *Electrical alternans and spiral wave breakup in cardiac tissue*, CHAOS, 4(3): (1994), 461-472.

[3] Lagarias, J. C.; Reeds, A. J.; Wright, M. H. Wright, P. E., *Convergence properties of the Nelder-Mead simplex method in low dimensions*, SIAM Journal of Optimization, 9(1): (1998), 112-147.

[4] Monteiro, E. C.; Lima, E. A.; Barbosa, C. H.; Ornelas, P. H.; Cavalcanti, E. G.; Santos, S. F.; Marchesin, D.; Plohr, B.; Gundelach, B.; Marchesin,

A.; Brio, M.; Ribeiro, P. C., *Magnetic localization of reentrant activation in isolated rabbit atrium*, Recent Advances in Biomagnetism; Takashi Yoshimoto, Makoto Kotani, Shinya Kuriki, Hiroshi Karibe and Nobukazu Nakasato. Tohoku University Press, Sendai: (1999), 1018-1021.

[5] Osppenheim, A. V.; Willsky, A. S., *Signals and Systems*, New Jersey, Prentice-Hall, 1983.

[6] Poty, H.; Saoudi, N.; Haissaguerre, M.; Daou, A.; Clementy, J.; Letac, B., *Radiofrequency catheter ablation of atrial tachycardias*, Am. Heart. J. 131, (1986), 481-489.

[7] Ribeiro, P. C.; Bruno, A. C.; Silva, P. L. S.; Barbosa, C. R. H.; Ribeiro, E. P.; Monteiro, E. C.; Costa, A. F., *Detection of reentry currents in atrial flutter by magnetocardiography*, IEEE Trans. Biomed. Eng. 39-8, (1992), 818-824.

Rodrigo W. dos Santos
IMPA
Estrada Dona Castorina 110
22460-320 Rio de Janeiro, RJ, Brasil
rodrigo@fluid.impa.br

Dan Marchesin
IMPA
Estrada Dona Castorina 110
22460-320 Rio de Janeiro, RJ, Brasil
marchesi@impa.br

Beata Z. F. B. Gundelach
IMPA
Estrada Dona Castorina 110
22460-320 Rio de Janeiro, RJ, Brasil
beata@fluid.impa.br

Juliana Valério
IMPA
Estrada Dona Castorina 110
22460-320 Rio de Janeiro, RJ, Brasil
juliana@fluid.impa.br